An Experimental Characterization of the Impedance and Spectral Content of Multistable Structural Responses During Dynamic Bifurcations

Benjamin A. Goodpaster
Department of Mechanical and Aerospace Engineering,
The Ohio State University,
Columbus, OH 43210

Ryan L. Harne[1]
Department of Mechanical and Aerospace Engineering,
The Ohio State University,
Columbus, OH 43210
e-mail: harne.3@osu.edu

The ability to predict multistable structural dynamics challenges the development of future high-performance air vehicles that will be subjected to extreme multiphysics loads. To aid in the establishment of methodologies that characterize the response states of harmonically excited multistable structures, a catalog of empirical and practical evidence is necessary. Recent research has suggested that evolving aspects of mechanical impedance metrics may be correlated with measurable quantities, although their relation to bifurcations of the dynamic response remains incompletely understood. Motivated to begin establishing such knowledge base, this research seeks to construct a library of experimental evidence from which to draw generalized insights on the impedance- and spectral-changing trends of multistable structures undergoing severe nonlinear response due to harmonic loading. A connection between vanishing real and imaginary components of impedance and dynamic bifurcations is uncovered. In the process, a technique to forecast dynamic bifurcations is articulated, which utilizes mechanical impedance measurements in real-time to monitor the susceptibility of postbuckled structural components to undergo dynamic bifurcations. An examination of higher-order harmonics of the dynamic responses further illuminates the nearness to bifurcations and may help classify the precise response regime. Thus, by correlating the real-time impedance and spectral response with analytical predictions, a future tool may be established for condition monitoring and diagnosis. [DOI: 10.1115/1.4039533]

1 Introduction

Future generation of high-performance, lightweight aircraft may provide significant advantages to many applications [1,2]. One of the long-standing challenges of such aerostructural formulation is that the acoustic, thermal, and mechanical loads [3] may stress the lightweight, slender aircraft components into postbuckled, multistable configurations [4]. For panel structures, such phenomenon is known as skin-buckling [5]. In response to diverse excitation energies, multistable structures may exhibit snap-through dynamics, which are large-amplitude oscillations between the stable static equilibria of the structure [6]. In addition to decreased fatigue life or structural failure [7], the large deflections of snap-through on aircraft panels may lead to performance and life degradation of the air-breathing propulsion systems [8,9].

Thus, the accurate prediction of snap-through dynamics is critical to the operation of future high-performance air vehicles. To this end, Culler and McNamara [10,11] and Matney et al. [12] have made advancements toward a simulation-based framework by which the complex multiphysics interactions may be investigated. Yet, the large computational costs incurred by numerical methods have encouraged researchers to probe the dynamics of lightly buckled bistable beams and postbuckled oscillators because the low-dimensional dynamic systems are favorable to obtain underlying insights associated with bifurcations and snap-through response through analytical methods. For example, Wiebe et al. [13] examined a single degree-of-freedom (DOF) Duffing-type oscillator to understand the conditions that cause a multi-DOF curved panel to exhibit snap-through buckling. Indeed, the numerous fields in which bistable oscillators may be employed and the relative simplicity of bistable platforms compared to more general multistable systems have led to established analytical methods to study and predict the dynamic responses of bistable systems [14–16].

On the other hand, it is difficult to generalize the methods of analysis for single-DOF systems to structures of higher dimension, such as for buckled panels, particularly when multiple nonlinearities are present [17] and when responses may be far from equilibria [18]. Seeking to address the challenge, recent advancements have been made in the analytical prediction of multi-DOF nonlinear systems using describing functions [19–21]. Yet, these methods rely on assumptions of input/output similarities and are thus inadequate to predict the coexistence of near-to- and far-from-equilibrium dynamic responses, such as the potential for either small excursions from equilibria or large amplitude snap-through in multistable structures.

To facilitate the analytical prediction of nonlinear dynamic responses potentially far-from-equilibria in multi-DOF systems, the authors recently proposed and validated a semi-analytical framework to solve the governing equations of motion when the systems are driven by harmonic inputs [22]. Moreover, the method obtains mechanical impedance metrics that provide insight on dynamic state integrity, including the onset of transition between coexisting dynamic responses [22]. While impedance has been used to study linear structural [23], electrical [24], and

[1]Corresponding author.

Contributed by the Technical Committee on Vibration and Sound of ASME for publication in the Journal of Vibration and Acoustics. Manuscript received August 16, 2017; final manuscript received February 13, 2018; published online April 20, 2018. Assoc. Editor: Miao Yu.

acoustic systems [25], it has not yet been widely used to study nonlinear structural systems. Approaches of evaluating receptance in harmonically driven nonlinear structures [16,26,27] provide a counterpart view to impedance. Yet, the use of mechanical impedance specifically helps identify energy transfer paths of built-up multistable structures. This becomes a potential means to characterize structural integrity in the vicinity of dynamic bifurcations due to the energy-based formulation, which is not revealed by receptance metrics. To enable such understanding, a comprehensive investigation of the newly identified energy management mechanisms observed in practice is required. Because of the challenges encountered to generalize ideal analytical insights to the context of practical multistable structures, a consistent set of experimental data to catalog such dynamic behaviors and observable impedance metrics is motivated.

This research meets the need by experimentally examining the impedance and frequency content of the dynamic response of a built-up multistable structure subjected to harmonic excitation, and characterizing such energy management metrics when the structural system undergoes dynamic bifurcations. The justification of close attention to the bifurcation events is that such sudden transitions into new dynamic regimes may be detrimental to any structural system in practice due to the increased local stresses associated with large amplitude deflections. Through the experimental studies undertaken in this report, methods to predict these dynamic regime changes in practice are articulated, which may aid in the real-time health monitoring of aerostructural systems when implemented in concert with modeling efforts [28].

The remainder of this paper is organized as follows: In Sec. 2, the archetypal multistable structure used in this research and the experimental methodology are described. Then, in Sec. 3, experimental evidence is presented and discussed in the context of mechanical impedance and response frequency characteristics. These observations are then used in Sec. 4 to articulate new methodologies that may be used to predict dynamic bifurcations in real time and distinguish between distinct dynamic regimes.

2 Experimental Platform and Methodology Description

A similar experimental system as that used in Ref. [22] is implemented in this research to characterize the impedance of built-up multistable structures subjected to harmonic excitation. This system is chosen since it is a low-order representation of a more realistic multistable structure while still allowing generalized insight to be uncovered. A schematic is given in Fig. 1. The system consists of three simply supported and elastically coupled beams. Each beam is lightly postbuckled via fine-threaded load screws that axially compress each beam so as to only induce the fundamental mode of buckling. The "beam 1" of the system is driven by the electrodynamic shaker (LDS V408, Brüel & Kjær, Nærum, Denmark). The slight post-buckling leads to oscillations with spatially distributed deflections proportional to the fundamental buckling mode. As such, dynamic behaviors that occur at frequencies other than the driving frequency of the shaker are associated with nonlinear harmonics of the fundamental, rather than with higher order vibration modes of the postbuckled beams.

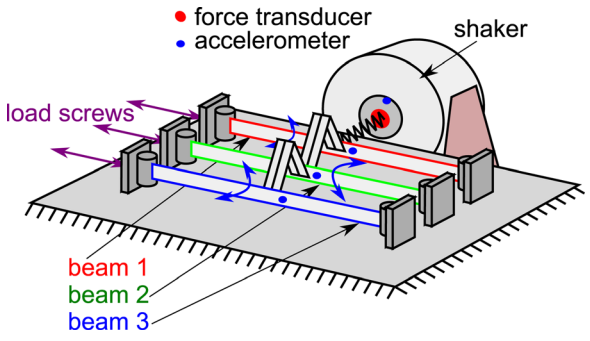

Fig. 1 Schematic of experimental platform employed in this research. Beam numbering denotes relative nearness to shaker.

Each beam is coupled to its nearest neighbor via a pair of leaf springs. The springs have clear influence on the potential dynamics that the system may exhibit. For instance, if the leaf springs are too compliant, only beam 1 will respond as driven by the shaker. In contrast, if the leaf springs are too stiff, all three beams will respond at nearly the same phase although only beam 1 is driven. The coupling leaf springs are, therefore, selected to facilitate a wide range of response dynamics. The coupling springs joining beams 1 and 2 (2 and 3) have a stiffness of 35 N/m (53 N/m). The spring stiffness between beam 1 and the shaker is 150 N/m. The remaining structural parameters of the platform, utilizing the same notation as Ref. [22], are given in Table 1.

An accelerometer (PCB 333B40, Depew, NY) and a force transducer (PCB 208C01) measure the acceleration and force input into beam 1. Miniature accelerometers (PCB 352A24) attached near the center of each beam measure the dynamic response of each beam. The shaker base acceleration output is governed by a vibration controller (Vibration Research VR9500, Jenison, MI) and subjects beam 1 to sinusoidal excitations with slowly varying excitation characteristics.

A particular contribution of this research is an investigation on differences between drive-point and transfer impedances when structural members undergo bifurcations. Mechanical impedance is determined by the ratio of excitation force to a response velocity. In analysis, the ratio is of complex, time-harmonic values, whereas experimental data employ the Fourier transforms of time series measurements. If the force and the velocity are measured at the same point, the ratio is a drive-point impedance. If the force and the velocity are not measured at the same point, the ratio is a transfer impedance. As a result, only one force transducer measuring the single external force on the system is required to calculate the impedance metrics presented in Sec. 3. In fact, any position, velocity, or acceleration sensor may be practically utilized in the characterization of impedance due to the time-harmonic nature of the metrics. Small accelerometers are used in this study for practical ease of fixturing and availability.

In this research, two types of harmonic shaker excitation are considered. Slow sweeps of varying base acceleration frequency with constant amplitude, termed "excitation frequency sweeps," are undertaken, along with slow sweeps using constant frequency with varying base acceleration amplitude, termed "excitation amplitude sweeps." This contrasts with the previous efforts [22], which focused exclusively on excitation frequency sweeps. Excitation frequency sweeps are conducted at a 0.05 Hz/s sweep rate with both an increasing and a decreasing excitation frequency and constant input amplitude, while excitation amplitude sweeps are conducted from at a rate of 0.0113 m/s^2/s, with both an increasing and a decreasing excitation amplitude. The sweep rates are chosen so as to induce quasi-steady-state dynamic responses. The constant amplitudes and frequencies for these experiments are selected to induce bifurcations in the experimental system for the sake of characterizing the impedance change near such critical points.

3 Experimental Results and Discussion

3.1 Energy Management Metrics During Bifurcations of Intrawell Dynamics. The first of the experimental results examined in this research are presented in Fig. 2. An excitation

Table 1 Experimentally measured structural parameters, utilizing the notation from Ref. [22]

Beam	m_i (g)	c_i (m N s/m)	$k_{i,i}$ (N/m)	$k_{NL,i,i}$ (MN/m^3)	p_i (dim)
1	15.1	134	222	159	2.44
2	15.1	130	222	86	2.21
3	15.1	87	222	497	2.12

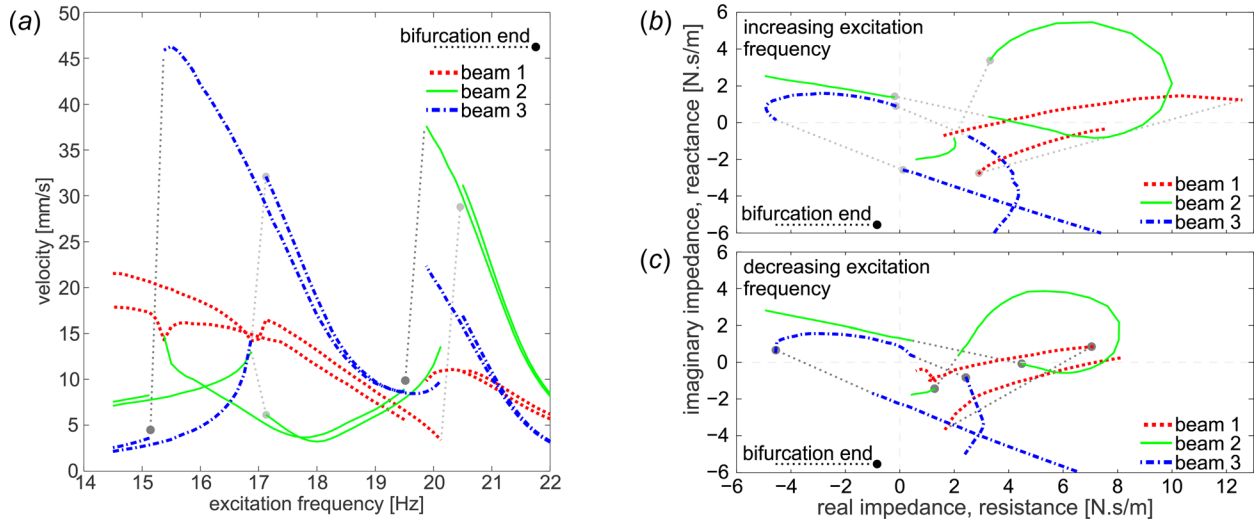

Fig. 2 Frequency sweep conducted at an excitation amplitude of 2.84 m/s^2. (*a*) Velocity amplitude response of all three beams with respect to excitation frequency. (*b*) and (*c*) Impedance measures for beams 1–3 with increasing and decreasing excitation frequency, respectively. Dashed lines with circular endpoints indicate transitions between distinct low-amplitude dynamic regimes. Light (dark) gray lines indicate increasing (decreasing) excitation frequency during bifurcation transitions.

frequency sweep is conducted with a base acceleration amplitude of 2.84 m/s^2, which induces a range of low amplitude, intrawell responses around the several statically stable equilibria. A fast Fourier transform converts the time-domain acceleration measurements to the frequency domain, which is then integrated in the time-harmonic sense to generate the velocity frequency response of each beam at the fundamental harmonic shown in Fig. 2(*a*). While the base acceleration amplitude of this experiment does not induce snap-through dynamics through driving beam 1, the excitation does induce dynamic bifurcations in the intrawell regime for all three beams, which occur near the linear natural frequencies due to softening of the primary resonances of the beam system. These natural frequencies are 16, 18, and 21.25 Hz. The bifurcation transitions are denoted in Fig. 2(*a*) by dashed lines with circular endpoints. Bifurcation transitions that occur during the increasing (decreasing) excitation frequency sweeps are denoted by light (dark) gray dashed lines, while the solid circular endpoint denotes the end of a dynamic bifurcation. The results shown in Fig. 2 are shown between 14.5 and 22 Hz, which is the frequency range wherein dynamic bifurcations occur. The largest response amplitude changes occur on beams 2 and 3. In addition, hysteresis effects lead the bifurcations about 2 Hz apart depending on whether the excitation frequency is increasing or decreasing in value. At the bifurcations occurring at 15 Hz and 17 Hz, during decreasing and increasing frequency sweeps, respectively, beam 1 enters a new steady-state dynamic with approximately the same amplitude. In contrast, beams 2 and 3 undergo more dramatic bifurcations that exhibit response amplitude changes by factors of 2.1 and 12.8, respectively.

Once the input force to beam 1 is converted into the frequency domain by a fast Fourier transform, the impedance of each beam is calculated by taking the ratio of the input force frequency response to the beam velocity frequency response [29]. When the velocity response and force are measured at the same (different) point, the result is termed drive-point (transfer) impedance. In this research, the impedance of beam 1 is drive-point, while those of beams 2 and 3 are transfer impedances. Figures 2(*b*) and 2(*c*) plot the impedances of beams 1–3 during increasing and decreasing excitation frequency sweeps, respectively. The plots use a standard convention of presenting the real (resistive) and imaginary (reactive) components of impedance in a parametric plane. Here, the parameter of change is the excitation frequency. To correlate between the frequency response of velocity in Fig. 2(*a*) and the parametric impedance plots in Figs. 2(*b*) and 2(*c*), the dashed lines denoting bifurcations in Fig. 2(*a*) also correspond to those dashed lines shown in Figs. 2(*b*) and 2(*c*).

By examining the impedance trends of each beam in Figs. 2(*b*) and 2(*c*), one notes that the reactance of all three beams vanishes near to the occurrence of each bifurcation. This is shown by the gray dashed lines crossing zero reactance. Since reactance corresponds to the effectiveness of energy exchange between a system component and the excitation in a manner analogous to exchange of kinetic and potential energies [29], it is determined that the intrawell dynamic bifurcations occur when a beam is no longer able to exchange so great of energy with the excitation force delivered to beam 1 and transmitted through the system. If the beams are unable to manage input energy effectively via damping or otherwise transferring energy to other DOF, the current steady-state dynamic becomes unstable and a dynamic bifurcation occurs. This vanishing reactance phenomenon during intrawell bifurcations was previously observed to occur for drive-point impedances [22] and is newly uncovered here in the parametric trends of transfer impedance.

Figure 3 displays the acceleration time series of the three beams (*a*) before and (*b*) after the bifurcation at approximately 20.25 Hz during the increasing excitation frequency sweep. This bifurcation event is denoted in Fig. 2(*a*) with a light gray dashed line and endpoint. Before the bifurcation, Fig. 3(*a*) shows that all three beams have similar amplitudes, while beam 3 oscillates almost 180 deg out of phase with beams 1 and 2. After the bifurcation, Fig. 3(*b*) shows that the amplitudes of the beams increase by 25%, 432%, and 127%, respectively. This is evident by the change in velocity response amplitude at the bifurcation occurring at 20.25 Hz in Fig. 2(*a*). There also appears to be a cascading effect in the beam responses, since each lags the previous beam in the series by approximately 90 deg seen in Fig. 3(*b*). This phenomenon is well known to occur for coupled oscillators when viscous damping is present, which underscores the fact that damping may be the primary energy management mechanism near intrawell bifurcations.

Looking more deeply into the spectral signatures of such dynamic bifurcations, Fig. 4 assesses the frequency content of the dynamics for the frequency up sweep from 14.5 to 22 Hz and frequency down sweep from 22 to 14.5 Hz. In Fig. 4, the amplitude of the short time Fourier transforms (SFFTs) of the beam acceleration measurements is shown in a logarithmic scale for ease of visualizing the contributions from other harmonics of the excitation

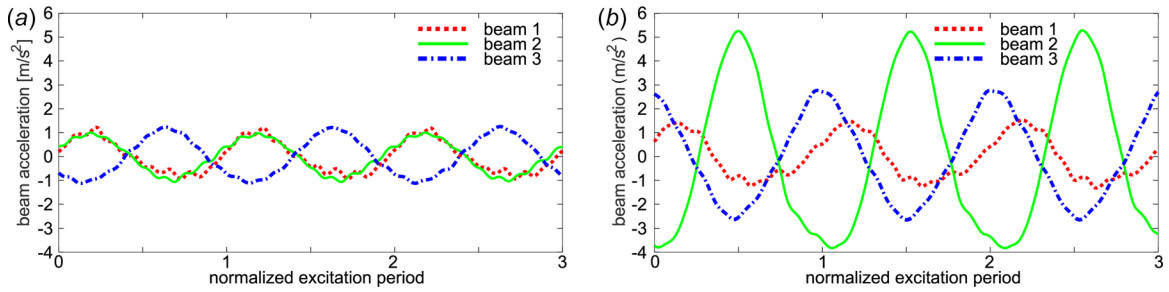

Fig. 3 Time series comparison (*a*) before and (*b*) after the dynamic bifurcation occurring at approximately 20.25 Hz with increasing excitation frequency

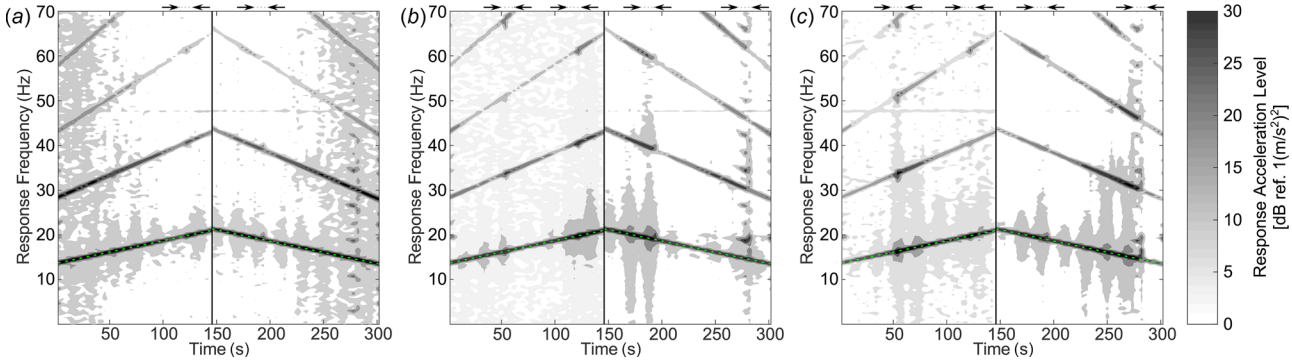

Fig. 4 (*a*)–(*c*) Short time Fourier transform of beam accelerations across the duration of the frequency sweep for beams 1–3, where the fundamental frequency responses are shown in Fig. 3. Arrows above each plot indicate locations of dynamic bifurcations. The excitation frequency is denoted via light dashed lines.

frequency as the experiment progresses. The excitation frequency is shown in Fig. 4 as a light dashed line. Since each beam responds at the same frequency as the harmonic driving force, the lowest dark line in the plots of Fig. 2 simultaneously corresponds to the excitation frequency and the fundamental harmonic of each beam response. Because the beams are seen to exhibit notable nonlinearity in the frequency response of Fig. 2(*a*), the spectral response in Fig. 4 confirms the existence of higher-order harmonics through the frequency sweep experiment, although at almost an order of magnitude or more less in amplitude than the fundamental. The point in the measurements at which the intrawell bifurcations occur is denoted in Fig. 4 with arrows above each plot.

Observing the plots in Fig. 4, it is seen that when the beams undergo intrawell bifurcations, denoted by the arrows above each plot, there is a temporarily large spillover of energy into higher-order harmonics. This is evident, for example, by the increase in the amplitude response level of the second harmonic of beam 2 from 23 dB to 31 dB as it undergoes the bifurcation at approximately 120 s, Fig. 4(*b*). Indeed, it is well known that multistable systems may exhibit higher-order harmonics on the same order of magnitude to that of the fundamental response [30]. It is confirmed here that such multiharmonic behavior becomes more greatly manifest at the onset of intrawell bifurcations.

The response amplitudes of the higher-order harmonics are also seen to increase starting around 200 s in Figs. 4(*a*)–4(*c*). This is particularly evident in beam 3 as it approaches the bifurcation at approximately 280 s in Fig. 4(*c*), corresponding to the bifurcation occurring at 15 Hz in Fig. 2(*a*). Such diffusion of input energy into higher-order harmonics may be one mechanism by which oscillators of a built-up, dynamic system manage injected energy when they may not effectively transfer the energy to neighboring oscillators or sufficiently dissipate it via damping mechanisms. On the other hand, in many instances, the amplitudes of the higher-order harmonics are one to two orders of magnitude smaller than the fundamental components. Indeed, higher-order harmonics are often excluded from analytical formulations due to the assumption that multiharmonic behavior is negligible [20]. Yet, the evidence presented here indicates that higher-order harmonics may be utilized as an indicator of highly nonlinear behavior, such as dynamic bifurcations, and should not be neglected in all instances.

3.2 Roles of Snap-Through on the Impedance and Spectral Metrics of Bifurcations. A subsequent experiment considers an increased excitation amplitude of 6.63 m/s^2. This amplitude of harmonic base acceleration is selected because it is found to induce snap-through dynamics for all three beams in certain ranges of the excitation frequency bandwidth. As seen in Fig. 5(*a*), the high-amplitude snap-through dynamic regime is prevalent at excitation frequencies of 10–14 Hz before the system transitions into a low amplitude response similar to that examined in Fig. 2(*a*). During the transition, a region of aperiodic response is observed from 14 to 17 Hz and has been excluded from Fig. 5(*a*) due to the attention in this research on steady-state dynamics pertinent to impedance metrics. As denoted by the gray dashed lines with endpoints in Figs. 5(*b*) and 5(*c*), the transition from snap-through to intrawell responses (and vice versa) corresponds to a vanishing reactance for both drive-point and transfer impedances. It is found that the vanishing reactance trend occurs regardless of whether the excitation frequency increases or decreases through the bifurcation. Indeed, this trend is also consistent with the intrawell bifurcations observed at higher excitation frequencies, which are denoted in Fig. 5 by gray dashed lines with endpoints with colors corresponding to the sweep direction. All together, the data establish the finding that bifurcations in the dynamic responses of each beam under frequency sweep excitation conditions correspond to vanishing drive-point and transfer reactances. Consequently, vanishing reactance, which is indicative

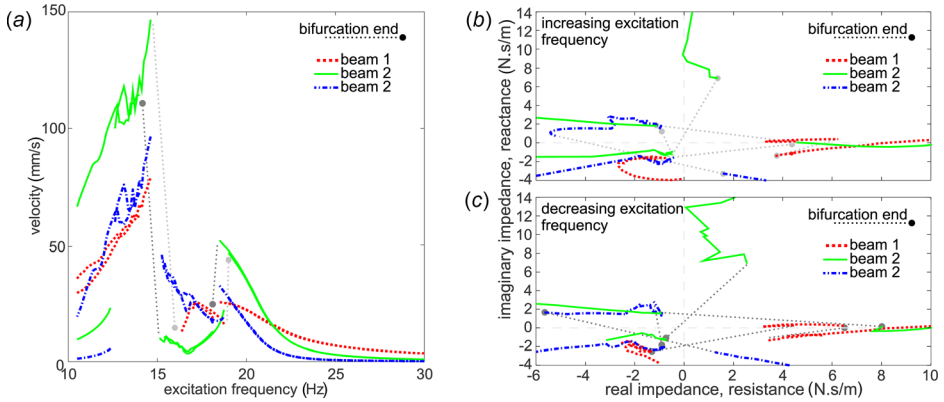

Fig. 5 Frequency sweep conducted at an excitation amplitude of 6.63 m/s^2. (*a*) Velocity amplitude response of all three beams with respect to excitation frequency. (*b*) and (*c*) Impedance measures for beams 1–3 with increasing and decreasing excitation frequency, respectively. Dashed lines with circular endpoints indicate dynamic bifurcations. Light (dark) gray lines indicate increasing (decreasing) excitation frequency during bifurcation transitions.

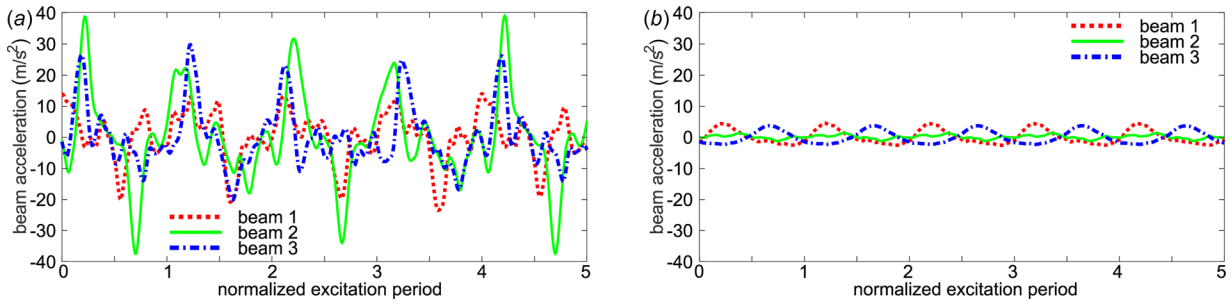

Fig. 6 Time series comparison (*a*) before and (*b*) after the transition from high-amplitude snap-through response to low amplitude intrawell response occurring at approximately 15 Hz

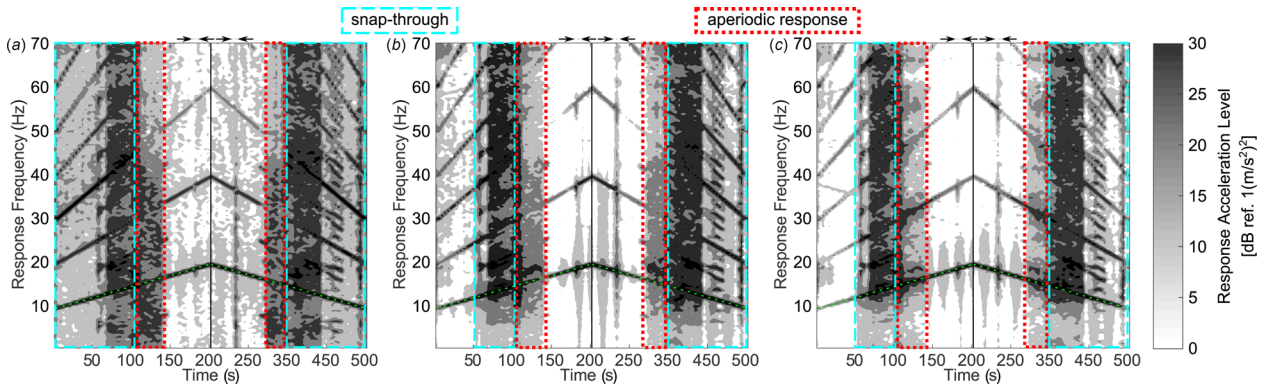

Fig. 7 (*a*)–(*c*) Frequency content of dynamic response across the duration of the experimental frequency sweep for beams 1–3. Arrows above each plot indicate intrawell dynamic bifurcations, while regions of snap-through and aperiodic response are denoted by dashed and dotted boxes, respectively. The excitation frequency is denoted via dashed lines.

of the inability to manage energy exchange locally at each DOF, results in the bifurcations. Such impedance change occurs regardless of whether the impedance is drive-point or transfer, and regardless whether the bifurcation event occurs between two intrawell states or between snap-through and intrawell dynamics.

The time series of beam accelerations (a) during and (b) after the snap-through dynamics with increasing excitation frequency, denoted by the light gray dashed line near 15–6 Hz in Fig. 5(*a*), are compared in Fig. 6. It is clear by examining the time domain response in Fig. 6(*a*) that higher-order harmonics significantly contribute to the snap-through oscillations for the multistable structure. Here in Fig. 6(*a*), it is seen that all beams are approximately in-phase, despite the existence of other-order harmonics. On the other hand, the intrawell responses in Fig. 6(*b*) are primarily sinusoidal at the drive frequency for beams 1 and 3, which oscillate around 180 deg out of phase with approximately the same amplitude, while beam 2 remains stationary by comparison.

Although the presence of other-order harmonics is clear from the time series of Fig. 6, the quantification of these contributions is made in Fig. 7. The frequency content of the short time Fourier transforms of the beam acceleration measurements in the bandwidth of 10–22 Hz are plotted in Fig. 7. Similar to Fig. 5, the

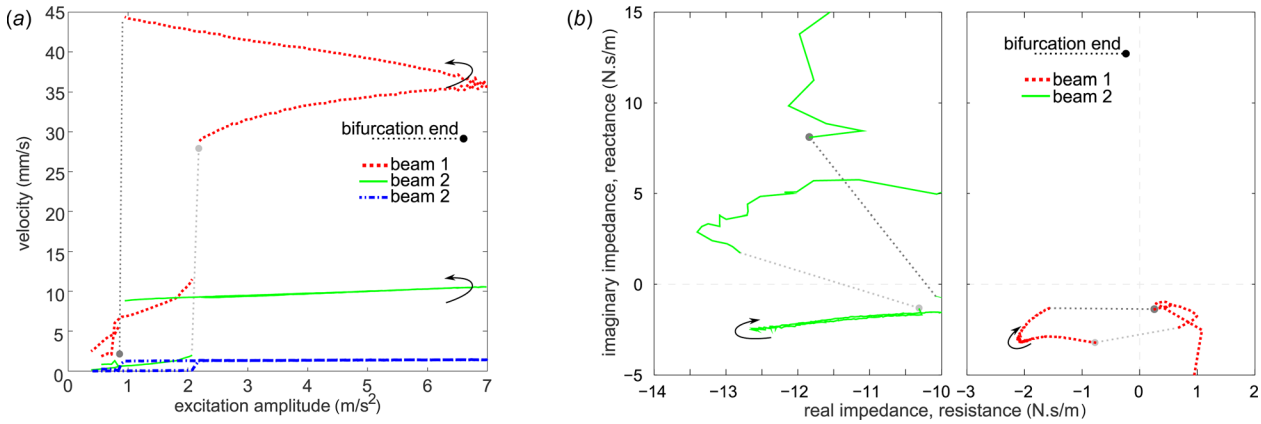

Fig. 8 Experimental amplitude sweep conducted at an excitation frequency of 11 Hz. (*a*) Velocity amplitude response of all three beams with respect to excitation amplitude. (*b*) Impedance measures for beams 1 (right) and 2 (left). Dashed lines with circular endpoints indicate dynamic bifurcations. Light (dark) gray markers indicate increasing (decreasing) excitation amplitude during bifurcation transitions.

excitation frequency is shown in Fig. 7 as dashed green lines. By examining the snap-through regions in Fig. 7, identified by blue dashed boxes, it is observed that snap-through dynamics exhibit a substantial spillover of energy into higher-order harmonics. In addition, a large broadband spillover into the frequencies between harmonics is evident during snap-through, in contrast to the intrawell regimes that have frequency content mostly restricted to only harmonics of the input base acceleration frequency. An exception to this is seen in the intrawell bifurcations denoted in Fig. 7 by the arrows above each plot, which also exhibit broadband frequency content of a greater level than the low excitation amplitude case examined in Sec. 3.1. This indicates that intrawell bifurcations exhibit an increase in frequency spillover effects for larger excitation amplitudes, while snap-through regimes exhibit persistent broadband frequency spillover. Thus, one may differentiate between interwell and intrawell responses by monitoring the frequency content of the dynamic responses of the members of a multistable structure. As indicated here, broadband frequency spillover characterizes interwell dynamics while, as noted in Sec. 3.1, frequency spillover to higher-order harmonics denotes a nearness to bifurcations when the prior dynamic state of the system is an intrawell regime.

3.3 Variation of the Energy Management as Harmonic Excitation Amplitude Changes. While the previous research efforts have examined the dynamic response of multistable structures subjected to harmonic excitation with slowly varying drive frequency [22], this research offers a first look into the impedance change trends resulting from excitation force having constant frequency and varying amplitude. Here, the experimental platform is excited at frequency 11 Hz. This is chosen based on the likelihood of inducing coexistent dynamics where bifurcations are manifest. Figure 8(*a*) examines the velocity amplitude frequency response at the fundamental harmonic of the base acceleration input, while (b) displays the impedance of beams 1 (right) and 2 (left). Note that due to the low amplitude dynamics of beam 3 without any large dynamic bifurcations throughout this experiment, as seen in Fig. 8(*a*), the impedance of beam 3 exhibits no discernable trends and is omitted.

Insight into the bifurcations of beams 1 and 2 with respect to impedance metrics may clearly be drawn. By comparing the velocity amplitude of beams 1–3 in Fig. 8(*a*) with respect to Fig. 5(*a*) at 11 Hz, it is observed that the response of beam 1 in Fig. 8(*a*) corresponds with a snap-through dynamic, while those of beams 2 and 3 are intrawell responses. The impedance trends of beam 2 indicate that the transfer reactance vanishes during dynamic bifurcations, shown by dashed lines with circular endpoints in Fig. 8(*b*), similar to the trends observed in the harmonic frequency sweep conditions. On the other hand, the drive-point resistance of beam 1 is seen to vanish during the transition between low and high amplitude responses. This contrasts with the vanishing reactance observed during excitation frequency sweeps. The vanishing resistance for beam 1 suggests that the bifurcations shown by dashed lines with circular endpoints in Fig. 8(*b*) are due to the inability of this DOF to transfer energy away or otherwise dissipate energy via damping mechanisms. The remaining internal exchange between potential and kinetic energy is insufficient to maintain the stability of the current steady-state dynamic. This reveals that driven members of a multistable structure may exhibit different primary energy management mechanisms depending on the varied excitation parameters.

The effects of higher-order harmonics are apparent when examining the short time Fourier transforms of the beam accelerations in Fig. 9. Note that because this experiment is conducted with a constant excitation frequency, the fundamental response frequency of each beam does not change, resulting in horizontal lines for all the harmonics of each beam. The large response amplitude of the second harmonic of beams 2 and 3 with respect to the fundamental harmonic, seen in Figs. 9(*b*) and 9(*c*) from the initial time to around 80 s, exemplifies multiharmonic diffusion. The response acceleration levels of the fundamental and second harmonics for beam 2 (3) around 80 s are 22 and 30 dB (10 and 26 dB), respectively. One also notes that the low-to-high amplitude bifurcations are characterized by the sudden onset of broadband frequency content, as seen in Fig. 9 at approximately 80 s and identified by the arrows shown above the plots. After such events, increased higher-order harmonic contributions are observed until the beam responses return to the low amplitude regime around time 570 s. At the initial bifurcation around 80 s as seen in Fig. 9(*a*), the third harmonic amplitude of beam 1 increases to 40 dB during snap-through, which is on the same order of magnitude as the fundamental harmonic (38 dB), while both the third and first harmonics are larger than the second harmonic (31 dB).

In contrast, the responses of beams 2 and 3 have large frequency content at each of the lowest three harmonics after the bifurcation, as shown in Fig. 9(*b*) and 9(*c*), respectively. For example, soon after the bifurcation around 80 s, the first, second, and third harmonic acceleration levels of beam 2 (3) are 31, 27, and 31 dB (23, 22, and 23 dB), respectively, revealing the relatively equal contributions from the harmonics to the total acceleration response. It is also observed that higher amplitude responses exhibit greater broadband frequency spillover, as exemplified by comparing the signal-to-noise ratios of 25 and 29 for beams 1 and 2, also noted in Fig. 9. These signal-to-noise ratios are computed by the ratio of the response acceleration level at 11 Hz to the

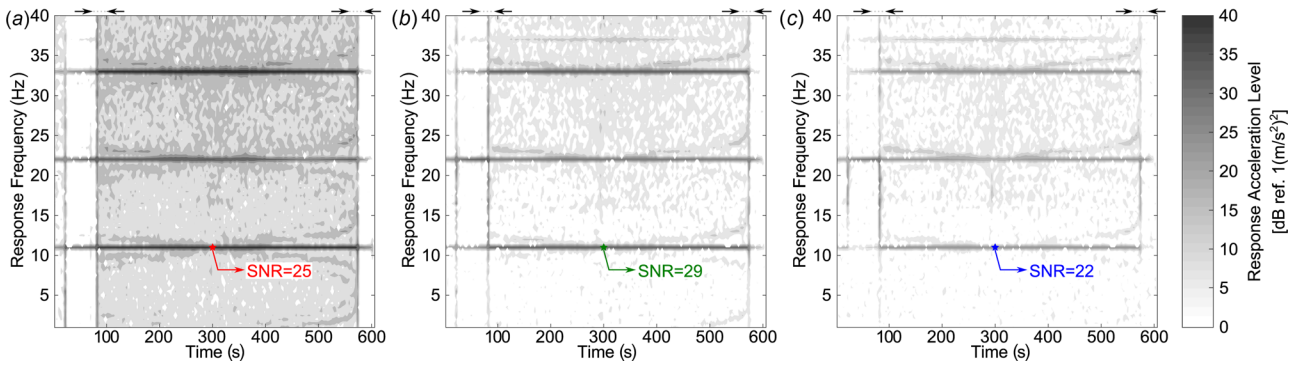

Fig. 9 (a-c) Frequency content of dynamic response across the duration of the experimental excitation amplitude sweep for beams 1–3. Arrows above each plot indicate dynamic bifurcations. The lowest order harmonic for all beams is 11 Hz, coincident with excitation frequency.

background levels of frequencies surrounding 11 Hz at 300 s. The results indicate that snap-through dynamics are characterized primarily by the first and third harmonics and relatively large amounts of broadband frequency spillover. This contrasts with intrawell responses that may have more equitable contributions from the lowest three harmonics but have much lower broadband energy spillover than snap-through cases in agreement with the previously noted trends [31,32].

4 Empirical Identification of Dynamic Bifurcations and Dynamic Regimes

These experimental results may inspire practical methods to forecast dynamic bifurcations according to the impedance and spectral characteristics of postbuckled structural components. For instance, velocity transducers may be placed at points on the multistable structure, while force transducers are placed at locations of known energy input, such as a bolted connection to adjacent structural members. In fact, any displacement or acceleration transducer may be used, provided the measurements are transformed into velocity data via the appropriate frequency domain differentiation or integration. The SFFTs of acquired data transform the signals from time to frequency domain. Then, the transformed measurements are used to calculate impedance. As such, the updated impedance metrics may be monitored for vanishing reactance or resistance. This research reveals that dynamic bifurcations may be forecast by the vanishing components of impedance, whether the measurement is of a drive-point or transfer impedance.

The SFFTs may concurrently be assessed for the spectral signatures of bifurcations. The evidence of energy spillover into higher-order harmonics or into frequencies surrounding the fundamental harmonic may be used to predict the onset of dynamic bifurcations from the response SFFTs, although this is not an absolute predictor as noted in Sec. 3.1. Yet, the spectral content of dynamic responses conclusively distinguishes between interwell and intrawell dynamic regimes. These methods may provide new tools to predict the onset of dynamic bifurcations and identify the dynamic regime of structures containing postbuckled constituents.

5 Conclusions

This research experimentally investigates the dynamic bifurcations of an archetypal multistable structure subjected to harmonic excitation frequency and amplitude sweeps. Specifically, measures of mechanical impedance and spectral content of the dynamic responses are examined. It is found that bifurcations of both drive-point and transfer oscillators undergoing excitation frequency sweeps correspond to vanishing mechanical reactance. When driven by excitation amplitude sweeps, the transfer reactance and the drive-point resistance vanish during bifurcations. This difference between observed trends for drive-point impedances indicates that the chosen variable excitation parameter leads to a difference in the evolution of the energy management mechanisms of the driven oscillator. A method to predict these bifurcations using real time measured structural responses and forces is proposed. It is generally observed that intrawell responses exhibit significant contributions from all three of the lowest-order harmonics. In contrast, snap-through dynamics exhibit large first and third harmonic orders in the response measurements and a larger extent of persistent broadband frequency spillover than intrawell regimes. Thus, monitoring the spectral content of structural systems may be used to determine the dynamic regime of the structure, thereby complementing the insight from the impedance metrics.

Acknowledgment

R .L. H. acknowledges start-up funds from the Department of Mechanical and Aerospace Engineering at The Ohio State University (OSU).

Funding Data

- U.S. Air Force Research Lab Summer Faculty Fellowship.
- U.S. Department of Defense Science, Mathematics, and Research for Transformation (SMART) Scholarship and the OSU College of Engineering Honors Research Scholarship.

References

[1] Walker, H. J., and Wolowicz, C. H., 1960, "Theoretical Stability Derivatives for the X-15 Research Airplane at Supersonic and Hypersonic Speeds Including a Comparison With Wind-Tunnel Results," National Aeronautics and Space Administration, Edwards, CA, Report No. NASA-TM-X-287.

[2] Kothari, A. P., and Webber, D., 2010, "Potential Demand for Orbital Space Tourism Opportunities Made Available Via Reusable Rocket and Hypersonic Architectures," AIAA Paper No. AIAA 2010-8600.

[3] Blevins, R. D., Bofilios, D., Holehouse, I., Hwa, V. W., Tratt, M. D., Laganelli, A. L., Pozefsky, P., and Pierucci, M., 2009, "Thermo-Vibro-Acoustic Loads and Fatigue of Hypersonic Flight Vehicle Structure," Air Force Research Laboratory, Wright Patterson Air Force Base, OH, Technical Report No. AFRL-RB-WP-TR-2009-3139.

[4] Spottswood, S. M., Eason, T. G., and Chona, R., 2013, "A Structural Perspective on the Challenges Associated With Analyzing a Reusable Hypersonic Platform," 11th International Conference on Recent Advancements on Structural Dynamics, Pisa, Italy, July 1–3, pp. 1–11.

[5] Soares, P. T. M. L., Monteiro, F. A. C., Neto, E. L., and Bussamra, F. L. S., 2013, "Skin Buckling of Fuselages Under Compression," 22nd International Congress on Mechanical Engineering (COBEM), Ribeirão Preto, Brazil, Nov. 3–7, pp. 8976–8985.

[6] Ng, C. F., 1989, "Nonlinear and Snap-Through Responses of Curved Panels to Intense Acoustic Excitation," J. Aircr., **26**(3), pp. 281–288.

[7] Przekop, A., and Rizzi, S. A., 2007, "Dynamic Snap-Through of Thin-Walled Structures by a Reduced-Order Method," AIAA J., **45**(10), pp. 2510–2519.

[8] Bolender, M. A., and Doman, D. B., 2005, "A Non-Linear Model for the Longitudinal Dynamics of a Hypersonic Air-Breathing Vehicle," AIAA Paper No. AIAA 2005-6255.

[9] Bolender, M. A., and Doman, D. B., 2006, "Modeling Unsteady Heating Effects on the Structural Dynamics of a Hypersonic Vehicle," AIAA Paper No. AIAA 2006-6646.
[10] Culler, A. J., and McNamara, J. J., 2010, "Studies on Fluid-Thermal-Structural Coupling for Aerothermoelasticity in Hypersonic Flow," AIAA J., **48**(8), pp. 1721–1738.
[11] Culler, A. J., and McNamara, J. J., 2011, "Impact of Fluid-Thermal-Structural Coupling on Response Prediction of Hypersonic Skin Panels," AIAA J., **49**(11), pp. 2393–2406.
[12] Matney, A., Mignolet, M. P., Culler, A. J., McNamara, J. J., and Spottswood, S. M., 2015, "Panel Response Prediction Through Reduced Order Models With Applications to Hypersonic Aircraft," AIAA Paper No. 2015-1630.
[13] Wiebe, R., Virgin, L. N., Stanciulescu, I., Spottswood, S. M., and Eason, T. G., 2012, "Characterizing Dynamic Transitions Associated With Snap-Through: A Discrete System," ASME J. Comput. Nonlinear Dyn., **8**, p. 011010.
[14] Harne, R. L., and Wang, K. W., 2017, *Harnessing Bistable Structural Dynamics: For Vibration Control, Energy Harvesting and Sensing*, Wiley, Chichester, UK.
[15] Virgin, L. N., 1985, "The Dynamics of Symmetric Post-Buckling," Int. J. Mech. Sci., **27**(4), pp. 235–248.
[16] Tang, B., and Brennan, M. J., 2015, "Steady-State Analysis of Nonlinear Systems by the Receptance Harmonic Balance Method," 22nd International Congress on Sound and Vibration, Florence, Italy, July 12–16, pp. 1–7.
[17] Peng, Z. K., Lang, Z. Q., Billings, S. A., and Tomlinson, G. R., 2008, "Comparisons Between Harmonic Balance and Nonlinear Output Frequency Response Function in Nonlinear System Analysis," J. Sound Vib., **311**(1–2), pp. 56–73.
[18] Khanin, R., Cartmell, M., and Gilbert, A., 2000, "A Computerised Implementation of the Multiple Scales Perturbation Method Using Mathematica," Comput. Struct., **76**(5), pp. 565–575.
[19] Tanrikulu, Ö., Bayindir, K., Özgüven, H. N., and İmregün, M., 1993, "Forced Harmonic Response Analysis of Nonlinear Structures Using Describing Functions," AIAA J., **31**(7), pp. 1313–1320.
[20] Elizalde, H., and Imregun, M., 2006, "An Explicit Frequency Response Function Formulation for Multi-Degree-of-Freedom Non-Linear Systems," Mech. Syst. Signal Process., **20**(8), pp. 1867–1882.
[21] Kalaycıoğlu, T., and Özgüven, H. N., 2014, "Nonlinear Structural Modification and Nonlinear Coupling," Mech. Syst. Signal Process., **46**(2), pp. 289–306.
[22] Harne, R. L., and Goodpaster, B. A., 2018, "Impedance Measures in Analysis and Characterization of Multistable Structures Subjected to Harmonic Excitation," Mech. Syst. Signal Process., **98**, pp. 78–90.
[23] Fahy, F., and Walker, J., 2004, *Advanced Applications in Acoustics, Noise, and Vibration*, Spon Press, New York.
[24] Callegaro, L., 2012, *Electrical Impedance: Principles, Measurement, and Applications*, CRC Press, Boca Raton, FL.
[25] Blackstock, D. T., 2000, *Fundamentals of Physical Acoustics*, Wiley, New York.
[26] Ren, Y., and Beards, C. F., 1994, "A New Receptance-Based Perturbative Multi-Harmonic Balance Method for the Calculation of the Steady State Response of Non-Linear Systems," J. Sound Vib., **172**(5), pp. 593–604.
[27] Budak, E., and Özgüven, H. N., 1993, "Iterative Receptance Method for Determining Harmonic Response of Structures With Symmetrical Non-Linearities," Mech. Syst. Signal Process., **7**(1), pp. 75–87.
[28] Glaessgen, E. H., and Stargel, D. S., 2012, "The Digital Twin Paradigm for Future NASA and U.S. Air Force Vehicles," AIAA Paper No. AIAA 2012-1818.
[29] Salter, J. P., 1969, *Steady-State Vibration*, Kenneth Mason, Havant, UK.
[30] Kostek, R., 2013, "An Analysis of the Primary and Superharmonic Contact Responances—Part 2," J. Theor. Appl. Mech., **51**(3), pp. 687–696.
[31] Harne, R. L., and Wang, K. W., 2014, "On the Fundamental and Superharmonic Effects in Bistable Energy Harvesting," J. Intell. Mater. Syst. Struct., **25**(8), pp. 937–950.
[32] Szemplińska-Stupnicka, W., and Rudowski, J., 1993, "Steady States in the Twin-Well Potential Oscillator: Computer Simulations and Approximate Analytical Studies," Chaos, **3**(3), pp. 375–385.